Scripta Materialia 211 (2022) 114530

Contents lists available at ScienceDirect

Scripta Materialia

journal homepage: www.elsevier.com/locate/scriptamat

Tunable femtosecond nonlinear absorption and optical limiting thresholds of La_2O_3–B_2O_3 glasses by controlling the borate structural units

G. Jagannath [a,b,*], Anuraag Gaddam [c,d], S. Venugopal Rao [e], D.A. Agarkov [f,g], G.M. Korableva [f], Manasi Ghosh [h], Krishna Kishor Dey [i], José M.F. Ferreira [c], Amarnath R. Allu [b,*]

[a] Department of Physics, Bangalore University, Bengaluru 560056, India
[b] Energy Materials and Devices Division, CSIR–Central Glass and Ceramic Research Institute, 196, Raja S C Mullick Road, Kolkata 700032, India
[c] Department of Materials and Ceramic Engineering, CICECO—Aveiro Institute of Materials, University of Aveiro, Santiago University Campus, Aveiro 3810193, Portugal
[d] São Carlos Institute of Physics, University of São Paulo, São Carlos, São Paulo 13566–590, Brazil
[e] Advanced Center of Research in High Energy Materials (ACRHEM), University of Hyderabad, Hyderabad, Telangana 500046, India
[f] Osipyan Institute of Solid State Physics RAS, 142432 Academician Osipyan str. 2, Moscow, Chernogolovka, Russia
[g] Moscow Institute of Physics and Technology, 141700 Institutskylane 9, Dolgoprudny, Moscow, Russia
[h] Physics Section, MMV, Banaras Hindu University, Varanasi, Uttar Pradesh 221005, India
[i] Department of Physics, Dr. Harisingh Gour Central University, Sagar, Madhya Pradesh 470003, India

ARTICLE INFO

Article history:
Received 23 November 2021
Revised 8 January 2022
Accepted 11 January 2022

Keywords:
Oxide glasses
Heavy metal oxides
Structural properties
Nonlinear optical
Structure–property correlations

ABSTRACT

Utilization of optical limiting materials to suppress the input intense laser energy is obligatory in a wide variety of applications that deploy the high–power laser sources. In this letter, we demonstrate that the optimization of borate structural units in lanthanum borate (LB) glasses through the addition of various concentrations of heavy metal oxides (HMOs) (PbO and Bi_2O_3) resulting in achievement of an optimum optical threshold value. The structural changes of these glasses were analyzed by ^{11}B MAS–NMR and Raman spectroscopic techniques. Nonlinear optical attributes were assessed by the Z–scan technique. The enhancement of two–photon absorption coefficient and decrement in optical limiting threshold factors suggest the LB glasses containing HMOs could be beneficial for power optical limiting devices. The achieved optical limiting threshold values of 0.075 and 0.114 J/cm^2 at 700 and 800 nm, respectively, are superior compared to advanced materials such as nanoparticles, carbon nanotubes, and few–layers of MoS_2/Polymethylmethacrylates.

Owing to the irrecoverable optical damages that occur upon using advanced high power laser sources, the demand for the development of laser safety devices such as optical limiting (OL) materials has been tremendously increased. OL materials mainly display third–order nonlinear optical (NLO) property and depict low limiting and high damage thresholds, fast response time, excellent transparency and broadband spectral protection [1–3]. Different classes of materials such as organo-polymers [4], carbon nanomaterials [5], organic dyes [6], graphene oxides [7], noble metal nanomaterials [8], inorganic crystals [9] and nano-composites [10] etc., have been widely studied for OL applications. Though excellent OL efficiencies are commonly observed in advanced materials, predicaments such as thermal decomposition, and low damage threshold hinder their practical use in the fabrication of devices. Owing to the good optical transparency over large spectral ranges, high damage threshold to irradiation, good thermal and mechanical stability [3,11], adjustable composition to meet the specific requirement, a special focus has been paid on the development of inorganic glass-based OL materials.

It is worth mentioning that NLO materials possessing strong nonlinear absorption (two–photon or multi–photon absorption) work as excellent optical limiters for different laser spectral regions and pulses [12,13]. Therefore, achieving high nonlinear absorption along with optical nonlinear susceptibility is becoming the primary criteria for obtaining efficient power optical limiters. Among different inorganic glasses of interest to date [11,14–18], the borate glasses have received significant interest. Due to the presence of different anionic borate units, the borate crystals whose NLO co-

* Corresponding authors at: Energy Materials and Devices Division, CSIR–Central Glass and Ceramic Research Institute, 196, Raja S C Mullick Road, Kolkata 700032, India.
E-mail addresses: jagannathgreddy@gmail.com (G. Jagannath), aareddy@cgcri.res.in (A.R. Allu).

https://doi.org/10.1016/j.scriptamat.2022.114530
1359-6462/

efficients are six times better than those of potassium dihydrogen phosphate crystals are being commercially used for NLO material [19]. It has been documented that borate systems containing planar six membered ring $(B_3O_6)^{3-}$ (connected with three BO_3 units) and the trigonal $(BO_3)^{3-}$ anionic groups with conjugated π–orbital systems are more favorable for achieving large NLO susceptibilities [20,21]. Further, the NLO susceptibility for $(BO_3)^{3-}$ units are in general four orders of magnitude higher than those of $(BO_4)^{5-}$ units (in borate crystals) [19]. It can therefore be anticipated that borate glasses containing a larger concentration of $(BO_3)^{3-}$ units demonstrate high optical nonlinearity. It has been reported that the addition of La_2O_3 to B_2O_3 glasses increases the concentration of $(BO_3)^{3-}$ units and their refractive index [22]. Several reports have documented that the incorporation of lead or bismuth in the borate glass network causes depolymerization of the glass structure and results in the formation of various borate units [23–25] by controlling the formation of BO_4 tetrahedron [26]. Further, the incorporation of heavy metal oxides (HMOs), in particular the PbO and Bi_2O_3, enhances the NLO attributes to several orders of magnitude [14,15,18,27–29]. In addition, the high polarizability values of Pb^{2+} (3.623 Å^3) and Bi^{3+} (1.508 Å^3) ions [30] and the elongated Pb–O and Bi–O bonds over shorter B–O bonds further contribute to the enhancement of NLO properties of glasses [31]. In the present letter, with the above background, we demonstrate a significant enhancement in the NLO coefficients of La_2O_3–B_2O_3 (LB) glass through the control of $(BO_4)^{5-}$ and $(BO_3)^{3-}$ units. The concentrations of $(BO_4)^{5-}$ and $(BO_3)^{3-}$ units in LB glass were altered with the addition of PbO or Bi_2O_3. The structural modifications, i.e., variations of BO_3 and BO_4 units, due to the incorporation of PbO or Bi_2O were assessed by ^{11}B magic angle spinning–nuclear magnetic resonance (MAS–NMR) spectroscopy, and NLO properties of the prepared glasses were assed using Z–Scan technique.

Glasses with the nominal composition (mol%) $10La_2O_3$–xHMO–$(90–x)B_2O_3$ ($30 \leq x \leq 50$, x is in steps of 10 mol% and HMO = PbO, Bi_2O_3) were synthesized by melt–quenching technique in porcelain crucibles using a resistive furnace in air atmosphere following the procedure reported elsewhere [27]. The prepared glasses were labeled as LPB–x and LBB–x for the glasses containing PbO and Bi_2O_3 respectively, in which x represents the concentration of PbO and Bi_2O_3 in corresponding compositions. The detailed glass synthesis procedure is provided in the supplementary information. The physical properties such as density (ρ) and refractive index (n) of glass samples were measured using Archimedes' principle and Abbes' refractometer, respectively. ^{11}B MAS–NMR spectra of glass samples were recorded on ECX 500 MHz JEOL NMR spectrometer. A 3.2 mm double–resonance MAS probe was employed with MAS frequency 18 kHz. ^{11}B frequency is quoted in ppm using ^{11}B NMR of 1 M H_3BO_3 (19.6 ppm) as reference. Raman spectroscopic measurements were performed by utilizing home–made setup explained elsewhere [32], the Raman spectra of samples were recorded by exciting with 532 nm laser. NLO properties were measured utilizing the Z–scan technique. The NLO properties were studied at spectral region from 700 to 1000 nm insteps of 100 nm utilizing ~150 (fs) laser pulses fired from Ti: sapphire laser at a repetition rate of 80 MHz. The detailed experimental procedures followed for ^{11}B MAS–NMR and Z–scan characterizations are described in the supporting information.

^{11}B MAS–NMR spectra for all the glasses are shown in Fig. 1a and 1b. The spectrum of each glass displays well resolved two broad peaks located at around ~ 15 ppm and ~ 1 ppm, which are the characteristic frequencies of BO_3 (B^3) and BO_4 (B^4) units, respectively [33]. The relative concentrations of BO_3 and BO_4 units and their relative isotropic chemical shifts in each glass are extracted using the deconvolution (Figs. S1 and S2 of supporting information) with the help of DMFit software and the corresponding parameters are tabulated in Table S1. Deconvolution of ^{11}B MAS–NMR spectra reveal that tetrahedral boron peak (B^4) centered around +1.01 ppm is resolved into two peaks namely $B^{4(1)}$ and $B^{4(2)}$. The trigonal boron peak centered around +15 ppm is also fitted to two peaks such as $B^{3(1)}$ and $B^{3(2)}$. From the Table S1 it is evident that the chemical shift of B^3 peaks shift slightly towards (relatively large shifting in Bi_2O_3 containing LB glass) the higher frequency, plausibly due to the variations in the environment of B^3 units [34]. The obtained asymmetry parameters for B^3 units clearly indicate that the BO_3 units in the present glasses contain one or two non–bridging oxygens (NBOs), which are indicated as BO_3^{NBO}. The variations of N_4 values, which are evaluated through the ratio of area under tetrahedral boron peaks to the total area under both trigonal and tetrahedral boron peaks, are represented in Fig. 1c with respect to HMOs content. It has been reported that in the case of binary alkali or alkaline–earth borate glass systems at a high concentrations (> 30 mol%) of alkali and alkaline–earths, the BO_3^{NBO} units increase at the expense of BO_4 units [35,36]. The appearance of broad vibrational bands at around 930 cm^{-1} and at 1300 cm^{-1} in the Raman spectra of LPB–40 and LBB–40 glass samples, (Fig. 1d) further confirm the presence of BO_3^{NBO} units. Similar Raman structural vibrational bands in the high frequency region have been observed for the Bi_2O_3–B_2O_3 and PbO–B_2O_3 glass systems [35,37,38]. According to the previous structural study on La_2O_3 containing borate glasses [22,39] the band observed at around 930 cm^{-1} is assigned to the symmetric stretching vibration of BO_3^{3-} groups (orthoborate groups [22]). A broad vibrational band near 1300 cm^{-1} is attributed to the pyroborate units. A strong vibrational band in 300 to 600 cm^{-1} range, which is characteristics peak of angularly constrained Bi–O–B linkages, in LBB–40 glass indicates that the Bi exist in the form of BiO_6 distorted octahedral unit [40]. Being an unconventional glass former (at lower concentrations), in most of the glass system, it is therefore assumed that Bi_2O_3 interacts with the borate network as a network modifier, whereas at high concentrations Bi_2O_3 prefers to retain the covalent nature as network builder through the formation of Bi–O–Bi bonds. Similarly, in PbO–B_2O_3 glass system, the lead attains PbO_4 and PbO_6 octahedral units at higher and lower concentrations of PbO, respectively. The Pb in its PbO_6 form behaves like a network modifier and interlinks with the BO_4 units, whilst the Pb in its PbO_4 form behaves as network former and forms the Pb–O–Pb linkages [35]. Lead in its PbO_4 form preferentially associates with BO_3 units rather than with the BO_4 units. Several studies [35,37] on structure of Bi_2O_3–B_2O_3 and PbO–B_2O_3 glasses reveal that Bi and Pb participate in the network structure through the Bi–O–B and Pb–O–B bonds. Therefore, considering the presence of various BO_3 units consisting NBOs (i.e., pyro, ortho and metaborates), it might be visualized that the BiO_6/PbO_6/PbO_4 units are distributed between the stacks of BO_3^{NBO} units and connected through the NBOs. Nevertheless, the presence of such connectivity needs to be confirmed. It is therefore understood that the increase in the concentration of Bi_2O_3 and PbO in the La_2O_3–B_2O_3 glass system increases the concentration of BO_3^{NBO} units which are further connected to the BiO_6/PbO_6/PbO_4 units. The Raman spectra of all the glass samples studied in the current work are provided in the supporting information (Fig. S3).

The variation of n with respect to PbO and Bi_2O_3 contents is presented in Fig. 1e. The compositional dependence of ρ and molar volume (V_m) as functions of PbO and Bi_2O_3 in La_2O_3–B_2O_3 glass is shown in Fig. 1f. From the Fig. 1f, it is evident that both ρ and V_m increase with an increase in HMOs. This behavior is attributed to higher atomic mass, larger atomic radii and longer bond length of PbO (223.2 a.m.u, 180 pm and 2.18–2.49 Å) and Bi_2O_3 (465.96 a.m.u, 160 pm and 2.08–2.80 Å) compared to that of B_2O_3 (69.62a.m.u, 85 pm and 1.38–1.53 Å). The increase in V_m is also attributed to the formation of NBOs with the addition of HMOs

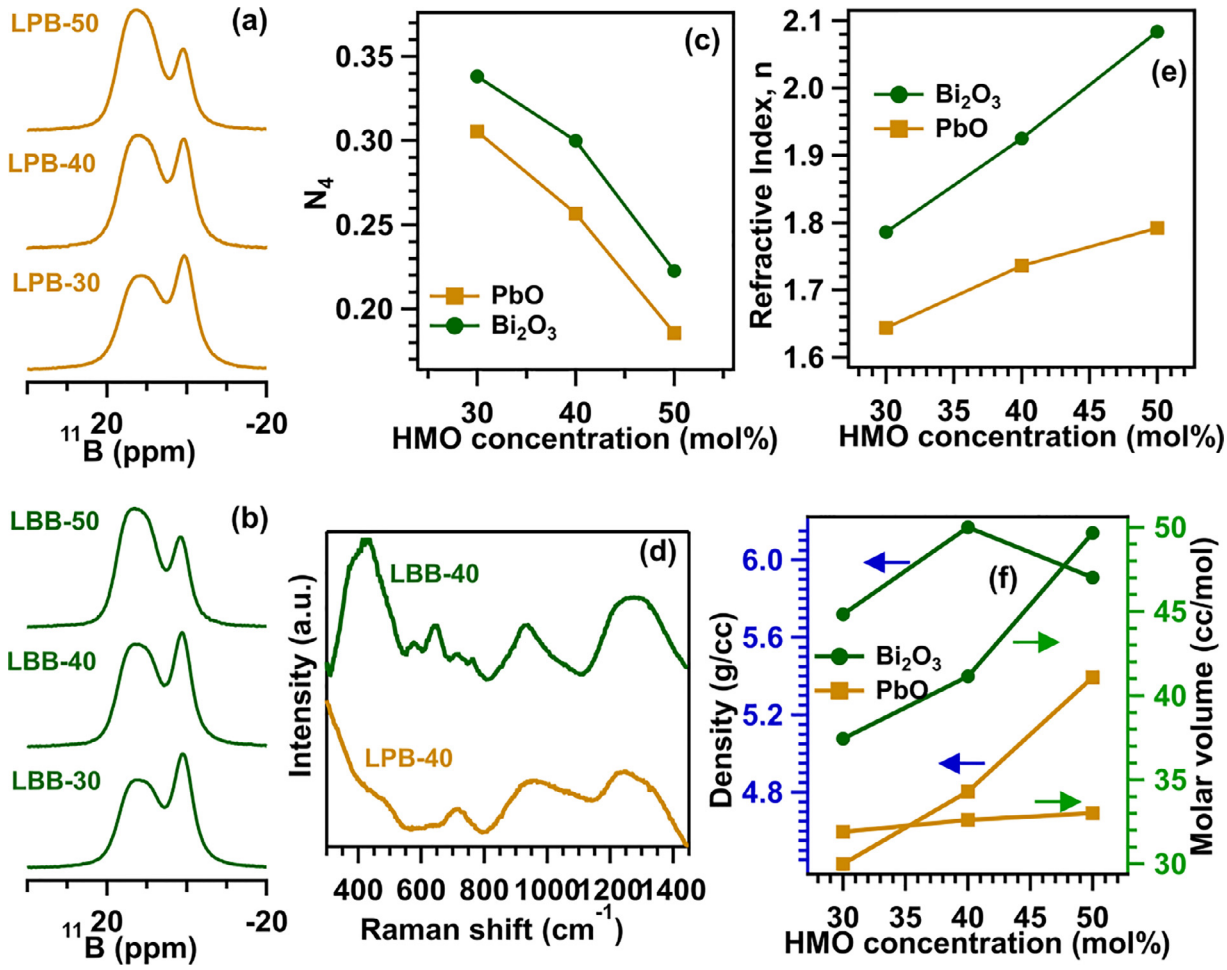

Fig. 1. ^{11}B MAS–NMR spectra of LB glass containing various concentrations of (a) PbO and (b) Bi_2O_3, (c) N_4 variation with respect to HMOs content in LB glasses, (d) Raman spectra of LPB–40 and LBB–40 glasses. Variations of (e) refractive index, and (f) density and molar volume with respect to the concentration of HMOs in LB glass.

[41,42] which is revealed by ^{11}B MAS–NMR and Raman spectral analysis. Nonetheless, a keen observation of density values of LBB–x glasses reveals a density reduction when Bi_2O_3 reached 50 mol%, i.e. for $Bi_2O_3 > 40$ mol% the density decreased. This anomalous behavior of density around $x = 40$ mol% could be understood because of the change in structural role from the modifier to network former. The increase in refractive index can be attributed to the high polarizability of heavy metal atoms and the NBOs [14]. The physical parameters such as molar electronic polarizability, molar refractivity values of all the glasses have been computed and furnished in Table S1.

Open–aperture (OA) and closed–aperture (CA) Z–scan measurements performed from 700 nm to 1000 nm for the La_2O_3–B_2O_3 glass containing HMOs and are shown in Fig. 2a and 2b, respectively. The data presented in Fig. 2a reveal that irrespective of the excitation wavelengths, all the glass samples depicted a decrease in transmittance as the sample moved towards the focal point. This indicates the existence of a reverse saturable absorption (RSA) mechanism in all the glasses used in the current study. To extract the nonlinear absorption coefficient, data were fitted with two photon absorption (2PA) equation [27,43] (solid lines in Fig. 2a) and the evaluated 2PA coefficients (α_2) for all the excitation wavelengths are represented in Fig. 3a. It is clear that α_2 increases with increasing the HMOs concentration in the LB glass. Typically, at 800 nm excitation, with increasing HMOs concentration the α_2 increases from 0.52×10^{-11} m/W to 0.99×10^{-11} m/W in LPB–x glasses and from 0.59×10^{-11} m/W to 1.08×10^{-11} m/W in LBB–x glasses as the HMOs content elevated from 30 to 50 mol%. The spectra in Fig. 2b reveal the signature of a valley–peak type, suggesting the presence of positive type nonlinearities ($n_2 > 0$) at all wavelengths of excitation. The phase shift ($\Delta\Phi$) [27] is evaluated from the data presented in Fig. 2b, where symbols represent the experimentally measured data and thick lines represent the theoretical fits. This positive nonlinear refraction could be attributed to self–focusing effect.

The procedure explained in Ref. [27] was followed to find the n_2 values and their variations with the composition as shown in Fig. 3b. Typically, at 800 nm irradiation, the n_2 increases from 0.43×10^{-18} m^2/W to 1.07×10^{-18} m^2/W and from 0.47×10^{-18} m^2/W to 1.09×10^{-18} m^2/W with increasing PbO and Bi_2O_3 content elevated from 30 to 50 mol%, respectively. Using α_2 and n_2 values, the real [Re $\chi^{(3)}$], imaginary [Im $\chi^{(3)}$], and total third order nonlinear susceptibility [$\chi^{(3)}$] values have been calculated using the relations mentioned in the Ref. [27] and resulted values are presented in Table 1. The improvement of $\chi^{(3)}$ as the function of HMO content is related to average bond lengths in glasses [27]. When PbO or Bi_2O_3 is incorporated for B_2O_3 in the LB glass, the number of elongated Pb–O bonds (the range of 2.18–2.49 Å) or Bi–O bonds (the range of 2.08–2.80 Å) [31,44] increases per unit volume, compared to that of shorter B–O bonds (the range of 1.38–1.53 Å) [31]. This results in an increase of the n_2 and hence $\chi^{(3)}$ with respect to HMOs content in the studied glasses.

The structural studies unveiled that the increase in the HMOs content in LB glass increases the formation of BO_3^{NBO} units. It has

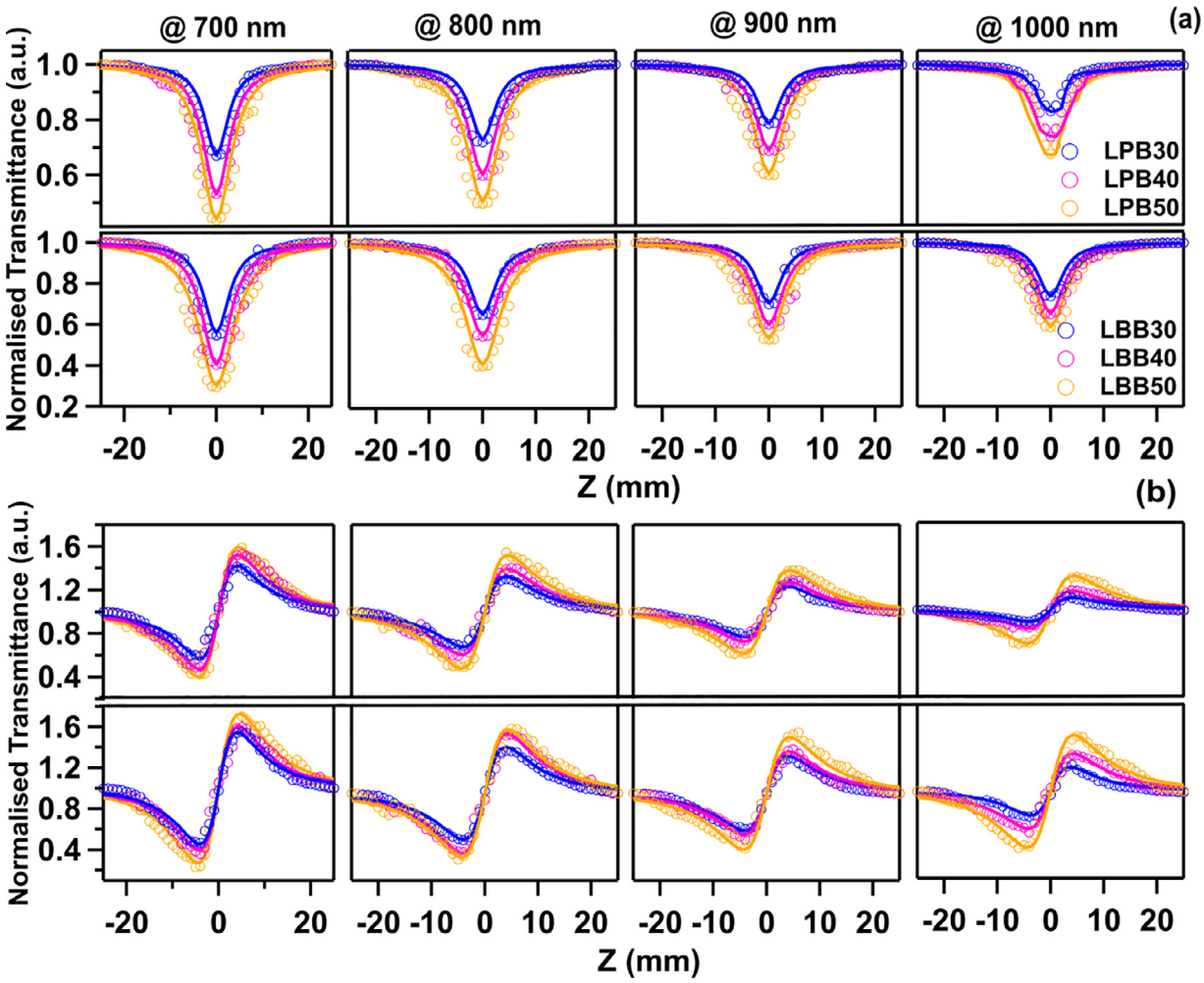

Fig. 2. Z–scan signatures, (a) Open aperture Z–scan, (b) closed aperture Z–scan profiles of PbO (upper profiles) and Bi_2O_3 (lower profiles) loaded LB glasses at all the excitation wavelengths. In the figures the symbols represent the experimentally collected data whilst the thick lines instantiate the theoretically fitted data.

been documented that the trigonal $(BO_3)^{3-}$ anionic groups possess larger electron population of the conjugated π–orbital system [19]. These π–orbital systems which made up of loosely held electrons can easily be distorted when exposed to high energy laser light. Normally, the NBOs are weakly bound to the network modifying cations and the valence electrons of the NBOs are easily distorted when subjected to a high intensity optical electric field. Raman spectral outcomes unveiled the distribution of $BiO_6/PbO_6/PbO_4$ units between the stacks of BO_3^{NBO} units and connected through the NBOs. The Pb^{2+} and Bi^{3+}ions possess [Xe] $4f^{14}$ $5d^{10}$ $6s^2$ electronic structure. Since the filled $4f^{14}$ $5d^{10}$ inner electronic shells screen the outer $6s^2$ electrons, the outer non–bonding lone electron pairs ($6s^2$) easily distort from the nucleus of Pb^{2+} and Bi^{3+} ions when excited with high intensity optical signal and thus permit larger charge displacements. Due to the combined charge displacements produced by π cloud, valence electrons of NBOs and non–bonding lone electron pairs ($6s^2$) of Pb^{2+} and Bi^{3+}causes the strong inharmonious effects thereby resulting in high optical nonlinearities in the studied glasses [26,31]. There are many literature reports explaining the role of lone pair of electrons on the enhancement in NLO coefficients of organic compounds and/or crystals [45–50]. Based on inferences, the interactions between the lone pair electrons on polarizable Bi^{3+} and Pb^{2+} cations and π–delocalized electrons on borate trigonal units are also responsible for the high optical nonlinearities observed in the studied glasses. Further, the molar refraction is related to the polarizability by the Lorenz–Lorentz equation. Also, the third–order nonlinear polarization is related to linear polarizability by fourth power. Therefore, larger the molar refraction larger the $\chi^{(3)}$ of the glasses. In oxide glasses the molar refraction sensitive to O^{2-} ions, are affected by neighboring cations. Increasing the ionic radius of the neighboring cations enlarges the molar refraction of glasses, because the ion refraction of the cation itself increases and the asymmetry of the electric field around the O^{2-} ion becomes large [51]. Therefore, when the PbO and Bi_2O_3 are incorporated in LB glasses cause enhancement in molar refraction due to the larger ionic radii of Pb^{2+} and B_i^{3+}ions compared to B^{3+} ions. Thereby, the polarizability of the substituted glasses consequently increases with increasing HMOs contents in LB glasses, which show enhanced $\chi^{(3)}$. From the Table S2, the electronic polarizability [52] values increase from 4.57 $Å^3$ to 5.55 $Å^3$ with increasing PbO content, and from 6.26 $Å^3$ to 10.73 $Å^3$ with increasing Bi_2O_3 concentration. This concludes that the enhancement in optical nonlinearity of the LPB–x and LBB–x glasses is also due to the high polarizability of $Pb^{2+}$and Bi^{3+}ions.

The ^{11}B MAS–NMR results revealed that the variations in the environment of B^3 units with increase of PbO and Bi_2O_3 contents and the asymmetry parameters indicate these BO_3 units contain NBOs. Also, from the Table S1 it can be seen that the area under trigonal boron peaks does not significantly increase with respect to HMOs content (instead, it is slightly decreasing). From the Raman spectral results, it is underlined that the $BiO_6/PbO_6/PbO_4$

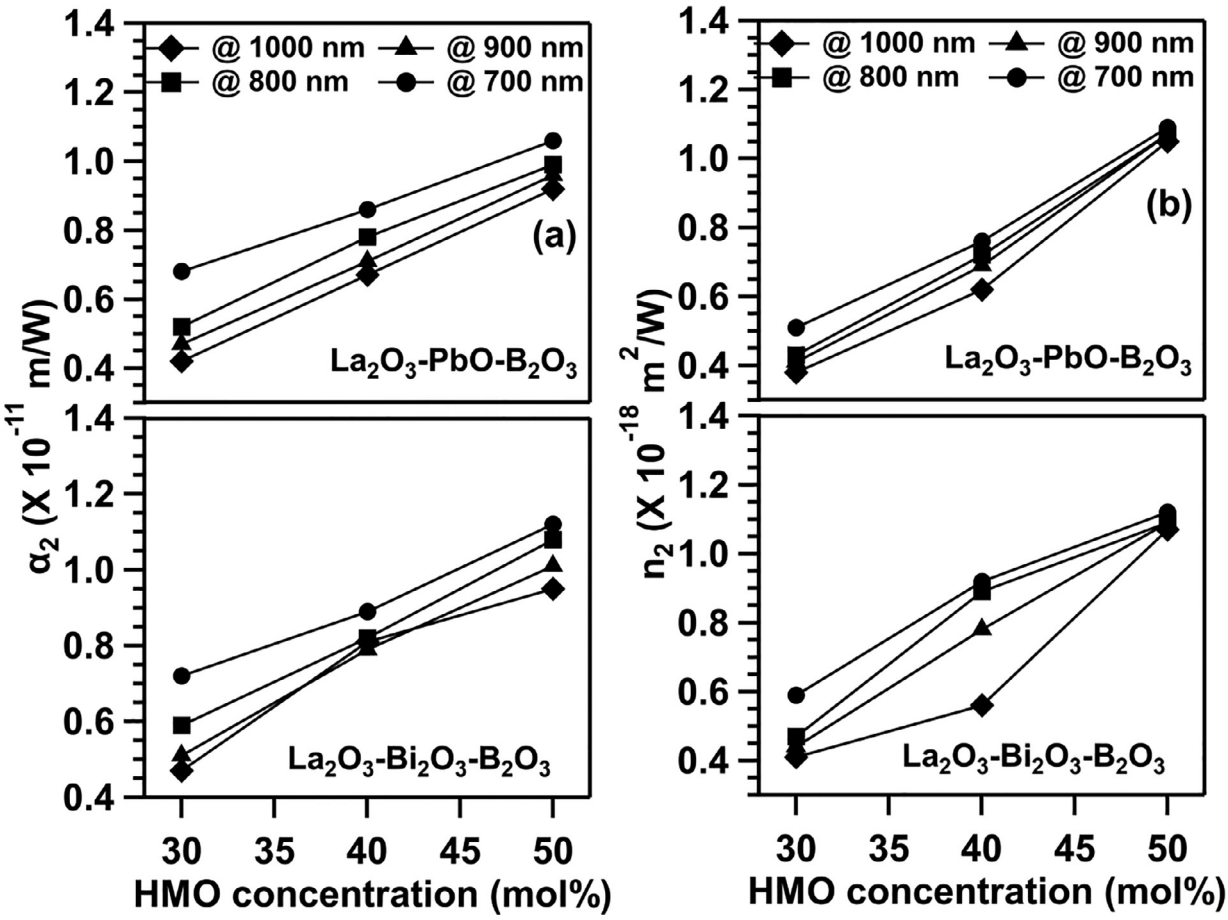

Fig. 3. Attenuation of (a) α_2 and (b) n_2 as the function of HMOs concentration in La_2O_3–B_2O_3 glasses.

Table 1
The real (*Re* $\chi^{(3)}$), imaginary (Im $\chi^{(3)}$), and total third order nonlinear susceptibility ($\chi^{(3)}$) of the glasses used in the current study at all the excitation wavelengths.

Sample codes	Re $\chi^{(3)}$ ($\times$ 10^{-13} esu)	Im $\chi^{(3)}$ ($\times$ 10^{-13} esu)	$\chi^{(3)}$ ($\times$ 10^{-13} esu)
λ = 700 nm			
LPB–30	3.499	2.599	4.358
LPB–40	5.812	3.666	6.872
LPB–50	8.883	4.814	10.103
LBB–30	4.776	3.248	5.775
LBB–40	8.651	4.664	9.829
LBB–50	12.344	6.879	14.132
λ = 800 nm			
LPB–30	2.949	2.272	3.722
LPB–40	5.507	3.800	6.690
LPB–50	8.719	5.139	10.121
LBB–30	3.805	3.042	4.871
LBB–40	8.369	4.912	9.704
LBB–50	12.013	7.582	14.206
λ = 900 nm			
LPB–30	2.812	2.309	3.639
LPB–40	5.277	3.891	6.556
LPB–50	8.719	5.606	10.366
LBB–30	3.561	2.958	4.630
LBB–40	7.335	5.323	9.063
LBB–50	12.013	7.976	14.420
λ = 1000 nm			
LPB–30	2.606	2.293	3.472
LPB–40	4.742	4.079	6.255
LPB–50	8.557	5.969	10.433
LBB–30	3.319	3.029	4.493
LBB–40	5.266	6.064	8.032
LBB–50	11.793	8.336	14.442

Table 2
The OL threshold values of studied glasses at all the excitation wavelengths, the table also enlists the OL threshold values of some recently reported advanced materials.

Sample codes /compositions	Excitation Wavelength and other experimental conditions	OL threshold values (J/cm^2)	Refs.
LPB–30	700 nm, 150 fs, 80 MHz	0.290	Present work
	800 nm, 150 fs, 80 MHz	0.344	
	900 nm, 150 fs, 80 MHz	0.415	
	1000 nm, 150 fs, 80 MHz	0.542	
LPB–40	700 nm, 150 fs, 80 MHz	0.190	
	800 nm, 150 fs, 80 MHz	0.229	
	900 nm, 150 fs, 80 MHz	0.305	
	1000 nm, 150 fs, 80 MHz	0.379	
LPB–50	700 nm, 150 fs, 80 MHz	0.135	
	800 nm, 150 fs, 80 MHz	0.171	
	900 nm, 150 fs, 80 MHz	0.231	
	1000 nm, 150 fs, 80 MHz	0.288	
LBB–30	700 nm, 150 fs, 80 MHz	0.210	
	800 nm, 150 fs, 80 MHz	0.279	
	900 nm, 150 fs, 80 MHz	0.315	
	1000 nm, 150 fs, 80 MHz	0.353	
LBB–40	700 nm, 150 fs, 80 MHz	0.120	
	800 nm, 150 fs, 80 MHz	0.203	
	900 nm, 150 fs, 80 MHz	0.235	
	1000 nm, 150 fs, 80 MHz	0.277	
LBB–50	700 nm, 150 fs, 80 MHz	0.075	
	800 nm, 150 fs, 80 MHz	0.114	
	900 nm, 150 fs, 80 MHz	0.190	
	1000 nm, 150 fs, 80 MHz	0.207	
Oleylamine–capped gold nanoparticles	780 nm, 300 fs, 10 Hz	26.0	[57]
Carbon nanotubes	780 nm, 300 fs, 10 Hz	10.0	
MoS_2/PMMA	800 nm, 100 fs, 1 Hz	315.1×10^{-3}	[58]
Au–Fe_2O_3–reduced graphene oxideCd–Fe_2O_3–reduced graphene oxide	700 nm, 150 fs, 80 MHz	26.60×10^{-6}	[59,60]
	800 nm, 150 fs, 80 MHz	26.29×10^{-6}	
	900 nm, 150 fs, 80 MHz 800 nm, 150 fs, 80 MHz	22.01×10^{-6} 0.65×10^{-6}	

units are distributed between the stacks of BO_3^{NBO} units and connected through the NBOs. Therefore, both the lone pair electrons from $Pb^{2+}$and Bi^{3+}ions and the conjugated π–orbital electrons of trigonal $(BO_3)^{3-}$ anionic groups are contributing for the enhancement of NLO coefficients. However, the intensity of high frequency Raman signals related to BO_3 units is decreasing and that of Raman signals related to Pb^{2+} and Bi^{3+} is increasing (majorly in Bi_2O_3 containing glasses) with PbO and Bi_2O_3 contents. This suggests that the contribution of lone pair electrons of Pb^{2+} and Bi^{3+}might be superior in comparison to that of conjugated π–orbital electrons of trigonal $(BO_3)^{3-}$ groups. Furthermore, $\chi^{(3)}$ of $20La_2O_3$–$80B_2O_3$ glass, which could be considered as similar to the pristine glass, was found to be 5.94×10^{-14} esu [53], being two orders of magnitude lesser when compared to highest value observed in the present study. This confirms the effective contributions of $Pb^{2+}$and Bi^{3+} cations along with BO_3^{NBO} units.

Generally, the optical limiter materials exhibit linear transmittance at lower input fluence and decrease the transmittance at greater input fluences [54]. The measurement of OL threshold evaluates the performance of OL materials. OL threshold is defined as the input laser intensity or fluence at which the transmittance or the intensity falls to 50% of the normalized transmittance [55]. Strong RSA and 2PA coefficients along with the nonlinear refraction mechanisms are responsible for inducing limiting action in materials [56]. In order to evaluate the OL threshold values with respect to HMOs content, the nonlinear transmission of all the glasses were estimated with respect to the input fluence and corresponding OL curves are displayed in Fig. 4. The OL thresholds values of LPB–*x* and LBB–*x* glasses are furnished in Table 2. The data in Table 2 indicate that the OL threshold decreases with increasing overall concentration of HMOs (PbO and Bi_2O_3) in the LB glass, confirming the enhancement in limiting efficiency. This enhancement in OL efficiency (decrease in OL threshold values) of LPB–*x* and LBB–*x* glasses is attributed to the strong 2PA and nonlinear refraction caused due to BO_3^{NBO}, Pb^{2+} (in LPB–*x*) and Bi^{3+} (in LBB–*x*) ions. The improvement in α_2 and decrement in OL threshold with respect to HMOs concentrations suggest that the glasses containing high content of HMOs beneficial for designing the high–power optical limiters to work in NIR region. The OL threshold values of some diverse material reported recently have been tabulated in the Table 2 along with experimental conditions. Table 2 data reveals that the LB glasses comprising HMO (50 mol%) are improved materials in contrast to advanced materials such as nanoparticles, carbon nanotubes and few–layer MoS_2/PMMA (PMMA: Polymethyl methacrylates, also known as acrylic glass), while the lowest OL threshold value achieved in the current study is greater in comparison to the graphene oxide materials [57–60].

The efficacy of HMOs (PbO and Bi_2O_3) on the structural and fs NLO properties of La_2O_3–B_2O_3 glasses has been investigated and discussed in detail. The ^{11}B MAS–NMR results revealed the decrease of BO_4 by increasing the BO_3 motifs. The Raman spectra confirm the existence and increase of pyro, ortho, and metaborate units in La_2O_3–B_2O_3 glasses with increase of HMOs content. The NLO features were improved in the studied glasses with respect to HMOs concentrations in the compositions. The enhancement in NLO features is attributed to the combined charge displacements produced by π electron cloud, valence electrons of O_2^{2-} and non–bonding lone electron pairs ($6s^2$) of Pb^{2+} and Bi^{3+}ions. The enhancement in n_2 is also attributed to an increasing number of elongated Pb–O and Bi–O bonds per unit volume. The OL threshold results are decreasing with enhancement in HMOs content in the composition. The 2PA and nonlinear refraction mechanisms are responsible for increasing the OL efficiency in the glasses. The enhancement of α_2 and decrement of OL threshold factors with respect to HMOs content suggest that the glasses encompassing high concentration of HMOs could be beneficial for fabricating power optical limiters to work in broad spectral wavelengths in the NIR region. Further, the OL threshold values also unveiled these glasses

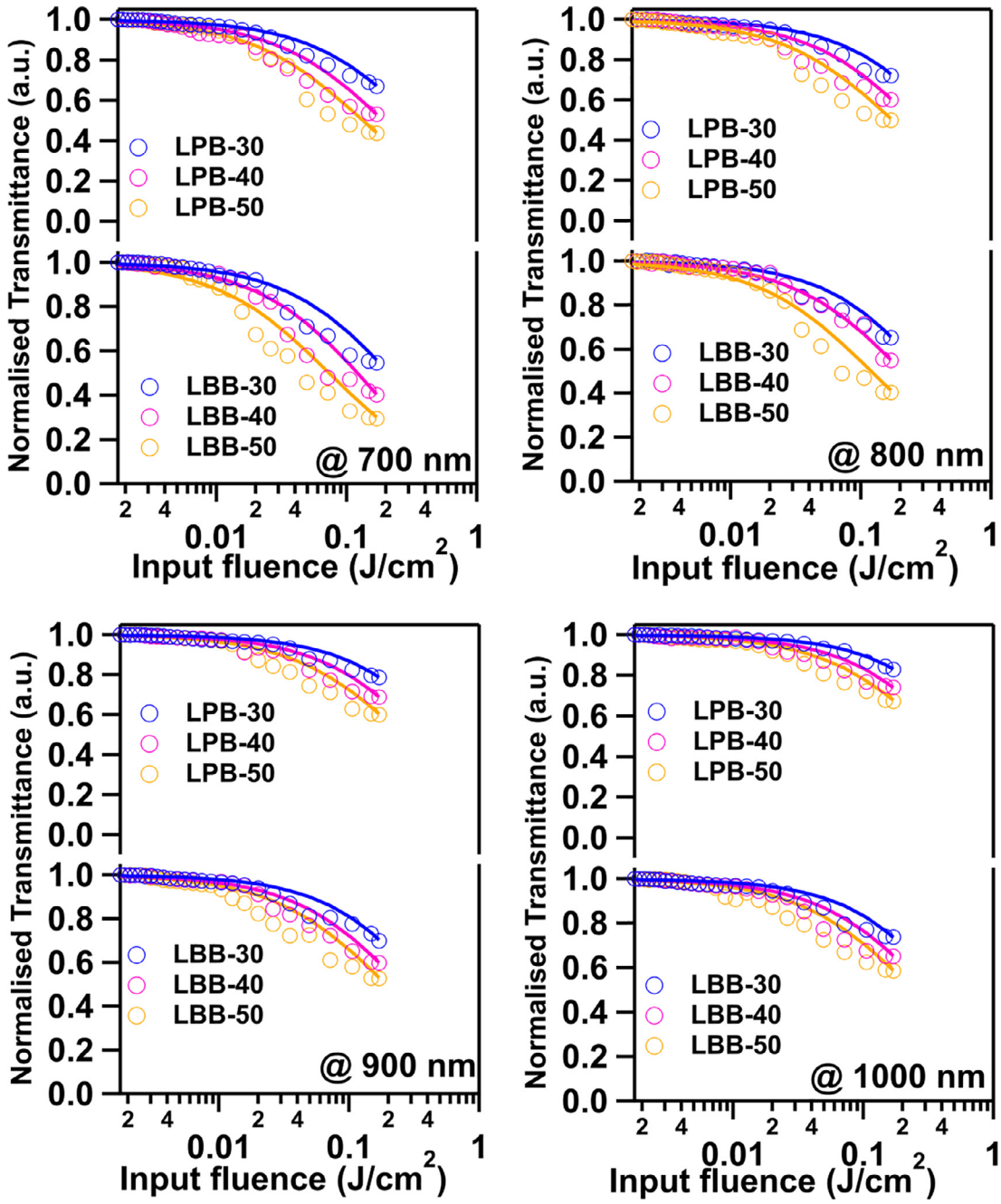

Fig. 4. Optical limiting profiles of LPB–*x* and LBB–*x* (where 30 ≤ *x* ≤ 50) glasses at all the excitation wavelengths, in the figures the symbols indicate the measured data points whereas the theoretical data represented by solid lines.

as competing materials in contrast to the advanced materials being investigated extensively.

Declaration of Competing Interest

The authors declare that they have no known competing financial interests or personal relationships that could have appeared to influence the work reported in this paper.

Acknowledgments

The authors (G.J) and (A.R.A) are thankful Dr. Suman Kumari Mishra, Director, CSIR–CGCRI and Dr. Abhijit Das Sharma, Head, Energy Materials and Devices Division, CSIR–CGCRI for their continuous support and encouragement. G.J would like to express his sincere gratitude to CSIR, New Delhi for providing the financial support in the form of CSIR–RA fellowship under the sanction number 31/015(0158)/2020–EMR–I. The author G.J. would like to thank Dr. B Eraiah, Professor, Department of Physics, Bangalore University, Bengaluru 560056 for providing early stage experimental facilities. S.V. Rao thanks DRDO, India for financial support through ACRHEM. Authors acknowledge the solid-state NMR facility of Sophisticated Instrument Center (SIC) of Dr. Harisingh Gour University, India. NMR spectra were also recorded using the NMR spectrometers which are part of the National NMR Network (PTNMR) and are partially supported by Infrastructure Project No. 022161 (co–financed by FEDER through COMPETE 2020, POCI and PORL and FCT through PIDDAC). This work was developed within the

scope of the CICECO-Aveiro Institute of Materials project, FCT Ref. UID/CTM/50011/2019. The authors D.A.A. and G.M.K. would like to thank the Russian Science Foundation grant 17–79–30071 for the financial support of Raman spectroscopy studies. A.G is grateful for the support from the São Paulo Research Foundation (FAPESP Processo n° 2021/06370–0) and CeRTEV (Center for Research, Technology, and Education in Vitreous Materials—process FAPESP n° 2013/07793–6).

Supplementary materials

Supplementary material associated with this article can be found, in the online version, at doi:10.1016/j.scriptamat.2022.114530.

References

[1] R.C. Hollins, Curr. Opin. Solid State Mater. Sci. 4 (1999) 189–196.
[2] L.W. Tutt, T.F. Boggess, Prog. Quantum Electron. 17 (1993) 299–338.
[3] Z. Xie, Y. Wu, X. Sun, S. Liu, F. Ma, G. Zhao, X. Hao, S. Zhou, Nanoscale 10 (2018) 4276–4283.
[4] J.W. Perry, K. Mansour, I.Y.S. Lee, X.L. Wu, P.V. Bedworth, C.T. Chen, D. Ng, S.R. Marder, P. Miles, T. Wada, M. Tian, H. Sasabe, Science 273 (80) (1996) 1533–1536.
[5] W.T. White, W.L. Smith, D. Milam, Opt. Lett. 9 (1984) 10.
[6] D. Château, Q. Bellier, F. Chaput, P. Feneyrou, G. Berginc, O. Maury, C. Andraud, S. Parola, J. Mater. Chem. C 2 (2014) 5105–5110.
[7] N. Liaros, E. Koudoumas, S. Couris, Appl. Phys. Lett. 104 (2014) 191112.
[8] R. Philip, P. Chantharasupawong, H. Qian, R. Jin, J. Thomas, Nano Lett. 12 (2012) 4661–4667.
[9] I.M. Pritula, A.V. Kosinova, O.N. Bezkrovnaya, M.I. Kolybaeva, V.M. Puzikov, A.V. Lopin, V.F. Tkachenko, M.A. Kopylovsky, V.O. Yatsyna, V.Y. Gayvoronsky, Opt. Mater. 35 (2013) 2429–2434.
[10] T.C.S. Girisun, M. Saravanan, S.Venugopal Rao, J. Appl. Phys. 124 (2018) 193101.
[11] S.Le Boiteux, P. Segonds, L. Canioni, L. Sarger, T. Cardinal, C. Duchesne, E. Fargin, G.Le Flem, J. Appl. Phys. 81 (1998) 1481.
[12] D. Dini, M.J.F. Calvete, M. Hanack, Chem. Rev. 116 (2016) 13043–13233.
[13] T. Wang, W. Huang, T. Sun, W. Zhang, W. Tang, L. Yan, J. Si, H. Ma, ACS Appl. Mater. Interfaces 12 (2020) 46565–46570.
[14] D. Manzani, C.B. de Araújo, G. Boudebs, Y. Messaddeq, S.J.L. Ribeiro, J. Phys. Chem. B 117 (2012) 408–414.
[15] Y. Chen, Q. Nie, T. Xu, S. Dai, X. Wang, X. Shen, J. Non Cryst. Solids 354 (2008) 3468–3472.
[16] F.E.P. dos Santos, C.B. de Araújo, A.S.L. Gomes, K. Fedus, G. Boudebs, D. Manzani, Y. Messaddeq, J. Appl. Phys. 106 (2009) 063507.
[17] R. Bala, A. Agarwal, S. Sanghi, N. Singh, Opt. Mater. 36 (2013) 352–356.
[18] H. Kanbara, K. Hirao, K. Tanaka, N. Sugimoto, S. Fujiwara, Y. Shimizugawa, J. Opt. Soc. Am. B 16 (1999) 1904–1908.
[19] R. Li, Crystal 7 (2017) 50.
[20] C. Chen, Y. Wu, R. Li, Int. Rev. Phys. Chem. 8 (1989) 65–91.
[21] F. Liang, L. Kang, P. Gong, Z. Lin, Y. Wu, Chem. Mater. 29 (2017) 7098–7102.
[22] A. Masuno, T. Iwata, Y. Yanaba, S. Sasaki, H. Inoue, Y. Watanabe, Dalton Trans. 48 (2019) 10804–10811.
[23] M. Veeramohan Rao, V.V. Ravi Kanth Kumar, N. Shihab, D. Narayana Rao, Opt. Mater. 84 (2018) 178–183.
[24] B.N. Meera, A.K. Sood, N. Chandrabhas, J. Ramakrishna, J. Non. Cryst. Solids 126 (1990) 224–230.
[25] Z. Pan, S.H. Morgan, B.H. Long, J. Non Cryst. Solids 185 (1995) 127–134.
[26] B. Karthikeyan, C.S.S. Sandeep, J. Cha, H. Takebe, R. Philip, S. Mohan, J. Appl. Phys. 103 (2008) 103509.
[27] G. Jagannath, B. Eraiah, A. Gaddam, H. Fernandes, D. Brazete, K. Jayanthi, K.N. Krishnakanth, S. Venugopal Rao, J.M.F. Ferreira, K. Annapurna, A.R. Allu, J. Phys. Chem. C 123 (2019) 5591–5602.
[28] T.R. Oliveira, K. Fedus, D. Manzani, E.L. Falcão–Filho, G. Boudebs, C.B. de Araújo, Y. Messaddeq, J. Appl. Phys. 108 (2010) 103523.
[29] B. Shanmugavelu, V.V. Ravi Kanth Kumar, R. Kuladeep, D. Narayana Rao, J. Appl. Phys. 114 (2013) 243103.
[30] V. Dimitrov, S. Sakka, J. Appl. Phys. 79 (1996) 1736–1740.
[31] P. Ramesh, V. Hegde, A.G. Pramod, B. Eraiah, S.V. Rao, S. Shisina, S. Das, D.A. Agarkov, G.M. Eliseeva, G. Jagannath, M.K. Kokila, Opt. Mater. 108 (2020) 110051.
[32] D.A. Agarkov, I.N. Burmistrov, F.M. Tsybrov, I.I. Tartakovskii, V.V. Kharton, S.I. Bredikhin, Solid State Ionics 302 (2017) 133–137.
[33] A. Bajaj, A. Khanna, B. Chen, J.G. Longstaffe, U.W. Zwanziger, J.W. Zwanziger, Y. Gómez, F. González, J. Non Cryst. Solids 355 (2009) 45–53.
[34] K. Januchta, R.E. Youngman, L.R. Jensen, M.M. Smedskjaer, J. Non Cryst. Solids 520 (2019) 119461.
[35] T. Takaishi, J. Jin, T. Uchino, T. Yoko, J. Am. Ceram. Soc. 83 (2000) 2543–2548.
[36] W.L. Konijnendijk, J.M. Stevels, J. Non Cryst. Solids 18 (1975) 307–331.
[37] C.P.E. Varsamis, N. Makris, C. Valvi, E.I. Kamitsos, Phys. Chem. Chem. Phys. 23 (2021) 10006–10020.
[38] G. Galleani, H. Bradtmüller, H. Fares, S.H. Santagneli, M. Nalin, H. Eckert, J. Phys. Chem. C 124 (2020) 25578–25587.
[39] S. Sasaki, A. Masuno, K. Ohara, Y. Yanaba, H. Inoue, Y. Watanabe, S. Kohara, Inorg. Chem. 59 (2020) 13942–13951.
[40] M. Dogra, K.J. Singh, K. Kaur, V. Anand, P. Kaur, P. Singh, B.S. Bajwa, Radiat. Phys. Chem. 144 (2018) 171–179.
[41] M. Subhadra, P. Kistaiah, Phys. B Condens. Matter 406 (2011) 1501–1505.
[42] S. Sindhu, S. Sanghi, A. Agarwal, V.P. Seth, N. Kishore, Mater. Chem. Phys. 90 (2005) 83–89.
[43] G. Jagannath, B. Eraiah, K. Jayanthi, S.R. Keshri, S. Som, G. Vinitha, A.G. Pramod, K.N. Krishnakanth, G. Devarajulu, S. Balaji, S.V. Rao, K. Annapurna, S. Das, A.R. Allu, Phys. Chem. Chem. Phys. 22 (2020) 2019–2032.
[44] Y.G. Choi, K.H. Kim, V.A. Chernov, J. Heo, J. Non Cryst. Solids 259 (1999) 205–211.
[45] W. Chen, Z.R. Li, D. Wu, F.L. Gu, X.Y. Hao, B.Q. Wang, R.J. Li, C.C. Sun, J. Chem. Phys. 121 (2004) 10489.
[46] R.L. Zhong, H.L. Xu, Z.R. Li, Z.M. Su, J. Phys. Chem. Lett. 6 (2015) 612–619.
[47] X. Shi, Q. Jing, Z. Chen, M.H. Lee, H. Duan, H. Ding, J. Appl. Phys. 128 (2020) 113104.
[48] R. Yin, C. Hu, B.H. Lei, S. Pan, Z. Yang, Phys. Chem. Chem. Phys. 21 (2019) 5142–5147.
[49] W. Cai, Q. Jing, J. Zhang, New J. Chem. 44 (2020) 1228–1235.
[50] K.M. Ok, Chem. Commun. 55 (2019) 12737–12748.
[51] H. Kanbara, K. Hirao, K. Tanaka, N. Sugimoto, S. Fujiwara, Opt. Lett. Vol. 21 (20) (1996) 1637–1639 1637–1639 21.
[52] G. Jagannath, B. Eraiah, K. NagaKrishnakanth, S. Venugopal Rao, J. Non Cryst. Solids 482 (2018) 160–169.
[53] K. Terashima, S. Tamura, S.–.H. Kim, T. Yoko, J. Am. Ceram. Soc. 80 (1997) 2903–2909.
[54] R. Divya, N. Manikandan, T.C. Sabari Girisun, G. Vinitha, Opt. Mater. 100 (2020) 109641 (Amst)..
[55] Z. Shi, N. Dong, D. Zhang, X. Jiang, G. Du, S. Lv, J. Chen, J. Wang, S. Zhou, J. Am. Ceram. Soc. 102 (2019) 3965–3971.
[56] D.H. Gu, F.X. Gan, W.F. Zhang, Y.Z. Gu, Opt. Lett. 26 (2001) 1788–1790.
[57] L. Polavarapu, N. Venkatram, W. Ji, Q.H. Xu, ACS Appl. Mater. Interfaces 1 (2009) 2298–2303.
[58] G. Liang, L. Tao, Y.H. Tsang, L. Zeng, X. Liu, J. Li, J. Qu, Q. Wen, J. Mater. Chem. C 7 (2019) 495–502.
[59] T.C.S. Girisun, M. Saravanan, V.R. Soma, A.C.S. Appl, Nano Mater. 1 (2018) 6337–6348.
[60] M. Saravanan, T.C.S. Girisun, S.V. Rao, J. Mater. Chem. C 5 (2017) 9929–9942.